The Cryosphere, 20, 7013–7021, 2026
https://doi.org/10.5194/tc-20-7013-2026
© Author(s) 2026. This work is distributed under
the Creative Commons Attribution 4.0 License.

The Cryosphere Open Access EGU

# Brief communication: The Interdecadal Pacific Oscillation is not a reliable indicator of the timing of an ice-free Arctic

**Christopher Wyburn-Powell and Alexandra Jahn**

Department of Atmospheric and Oceanic Science and Institute of Arctic and Alpine Research, University of Colorado Boulder, Boulder, Colorado.

**Correspondence:** Christopher Wyburn-Powell (chwy8767@colorado.edu)

Received: 13 April 2026 – Discussion started: 21 April 2026
Revised: 19 September 2026 – Accepted: 5 October 2026 – Published: 27 November 2026

**Abstract.** The Arctic is transitioning towards a seasonally ice-free state over the next few decades, with internal variability determining precisely when. The phase of the Interdecadal Pacific Oscillation (IPO) has been proposed to reduce internal variability uncertainty in ice-free predictions. Using eight large ensembles from the Coupled Model Intercomparison Project – Phase 5 (CMIP5) and CMIP6, starting from current mean sea ice extent, we find no agreement that the IPO affects ice-free timing. However, a majority of large ensembles indicate the IPO can affect the rate and spatial distribution of Arctic sea ice decline over the next two decades.

## 1 Introduction

Arctic sea ice is projected to rapidly decline over the next few decades, likely becoming seasonally ice-free by mid-century, independent of emissions scenario (Notz and SIMIP-Community, 2020; Årthun et al., 2021; Jahn et al., 2024). Internal climate variability drives large variations in sea ice trajectory over interannual to decadal timescales (Kay et al., 2011; Wettstein and Deser, 2014; Swart et al., 2015; Bonan et al., 2021). Single-model initial condition large ensembles (LEs) can isolate the contribution of internal variability (Fasullo et al., 2020). The timing of an ice-free Arctic can vary by over two decades depending solely on the climate realization (Notz, 2015; Jahn et al., 2016), with this simulated range of internal variability differing somewhat between LEs and ice-free definitions (Holland and Hunke, 2022; Jahn et al., 2024). Thus, understanding the predictability and magnitude of internal variability at decadal timescales can potentially help reduce projection uncertainty of ice-free conditions.

The Interdecadal Pacific Oscillation (IPO) is a leading driver of climate variability on multi-decadal timescales (Vance et al., 2022). Screen and Deser (2019) showed that the IPO phase at mean sea ice extent states similar to today's affects the time of a consistently ice-free Arctic by 9 years, using the Community Earth System Model version 1 (CESM1). In that study, the transition from a negative to positive phase of the IPO was associated with a persistent strengthening of the Aleutian Low in CESM1, favoring enhanced poleward heat and moisture transports, facilitating faster Arctic sea ice loss. However, the teleconnection between the IPO and Arctic sea ice has received little direct attention. Where this teleconnection was examined, the IPO was shown to be the largest driver of sea ice concentration from a suite of climate modes of variability, with its impact focused in the Beaufort and East Siberian Seas at 5–15 year lead times (Wyburn-Powell and Jahn, 2024). The related Pacific Decadal Oscillation has also been linked to Arctic sea ice variability (Kim et al., 2020; Simon et al., 2022).

Assessing whether the IPO can reduce internal variability uncertainty in projections of consistently ice-free conditions requires examining multiple global climate models, given the varying realism of Pacific–Arctic teleconnections across Coupled Model Intercomparison Project – Phase 5 (CMIP5) and CMIP6 models (Topál et al., 2020; Jahfer et al., 2024). Furthermore, isolating the influence of the IPO on Arctic sea ice requires a large sample of ensemble members, due to infrequent samples of this low-frequency mode of variability. This is compounded by the possibility of non-stationary transmission of tropical Pacific sea surface tem-

perature anomalies to Arctic geopotential height and sea ice anomalies (Ding et al., 2014; Baxter et al., 2019; Bonan and Blanchard-Wrigglesworth, 2020). Finally, because CMIP5 and CMIP6 models inconsistently reproduce the IPO's observed spatial pattern, amplitude, and phase evolution (Qin et al., 2024), detection of relationships between the IPO phase and Arctic sea ice is further complicated.

To assess the reliability of the IPO to reduce the prediction uncertainty of a consistently ice-free Arctic, here we use eight LEs with at least 30 members, two from CMIP5 and six from CMIP6 (Table 1). The CMIP5 models include the CESM1 used in Screen and Deser (2019), to allow for direct comparison of other models to earlier results.

## 2 Data and Methods

### 2.1 Data

We use eight climate models which provide large ensembles (LEs) for our analyses, see Table 1. The LEs used are those from CMIP5 and CMIP6 which provide at least 30 ensemble members with output sufficient to obtain sea ice concentration, sea ice extent (SIE), and the IPO phase over both the historical and future scenario (RCP 8.5 or SSP3-7.0). Five of the six CMIP6 models used in this analysis were shown by Jahfer et al. (2024) to have strong Pacific-Arctic teleconnections: ACCESS-ESM1-5, CanESM5, CESM2-LENS, EC-Earth3, MPI-ESM1-2-LR; only MIROC6 was shown to have a weak (asymmetric) Pacific-Arctic teleconnection (CMIP5 models were not assessed in Jahfer et al., 2024). IPO simulation skill has been assessed for all models used here except for EC-Earth3 (Qin et al., 2024), with model skill ranging from 1st (CESM2-LENS) to 45th (ACCESS-ESM1-5) place from 52 models assessed (Table 1). In terms of their sea ice simulation, the eight LEs vary across common sea ice realism metrics such as forced response and September mean sea ice area (Table 1). For mean historical September sea ice area, 5 of the 8 models are within the uncertainty range from observational estimates, with three (CESM2-LENS, MPI-ESM1-2-LR, and CanESM5) below the observational estimate (Table 1). The sea ice area loss per degree of global warming is below the observed estimate in all models except CESM2-LENS, which agrees with the observed estimate (Table 1). Based on all of these model metrics relevant for this study, no model subset emerges as clearly superior for the purpose of detecting an influence of the IPO on the timing of an ice-free Arctic. Thus, we analyze all 8 ensembles in the following. Given the difference in results we find, it remains an open question which of these models, if any, does indeed capture reality most closely.

For observations, we use the National Snow and Ice Data Center (NSIDC) sea ice index (Fetterer et al., 2017) as observed SIE. Observed sea surface temperatures, used for calculating the IPO, are from HadISST (Rayner et al., 2003).

### 2.2 Methods

We assess projections of consistently ice-free conditions (Jahn et al., 2024), by defining the ice-free year as the first year the 11-year centered mean September SIE drops below 1 million $km^2$, following Screen and Deser (2019). The IPO is calculated using the Henley et al. (2015) tri-polar index of annual sea surface temperature anomalies, with low-frequency variability isolated by applying a zero-phase, 11-point Lanczos filter window via forward-backward filtering (`scipy.signal.filtfilt`) following the method in the Climate Variability Diagnostics Package (Phillips et al., 2014). For observational data, the centered 11-year mean is necessarily lagged by six years relative to the current state, since future observations are unavailable. The observational 11-year centered mean September SIE was 4.7 million $km^2$ in 2011 (as used for Screen and Deser, 2019), decreasing to 4.6 million $km^2$ in 2019 (Fetterer et al., 2017). From the 11-year centered mean SIE of 4.7 million $km^2$ in 2011, the selected CMIP5 and CMIP6 LEs project a range of 25–43 years until consistently ice-free conditions, with a mean of 33 years. Updated to the most recent September 2019 11-year centered mean SIE of 4.6 million $km^2$, the mean duration to consistent ice-free conditions reduces slightly to 32 years.

For our initial analysis of the influence of the IPO (Fig. 1) we follow the methodology of Screen and Deser (2019). This involves selecting all members starting at an 11-year mean SIE of 4.7 million $km^2$ and classifying their IPO phase based on 0.9 standard deviations from the mean. Statistical significance is calculated at the 95 % level using a Student's $t$-test based on the difference in the mean SIE between the positive and negative IPO groups of trajectories.

To incorporate multiple mean states, for each ensemble member we select 11 trajectories at 4.2–5.2 million $km^2$ at 0.1 increments. This has the effect of repeating the Screen and Deser (2019) method for 11 mean states before averaging to a single set of "pooled" trajectories for each LE as displayed in Fig. 2. For analyses where we "pool" initial sea ice states in Sect. 3.1, we classify the IPO phase based on persistence above/below zero for 10 years. This persistence criterion is chosen both to capture the typical IPO phase transition timescale and to be consistent with the current persistently negative phase (Henley et al., 2015). Significance testing for the pooled IPO states is tested by whether the IPO phase means are different from the ensemble mean at the 95 % level. Significance testing uses the number of LE ensemble members as independent samples, not the multiple samplings of the same ensemble member.

For the correlation analysis (Sect. 3.2) we compute correlations at lead times of 0 to 45 years prior to the ensemble-mean ice-free year. For each ensemble member for a given lead time, we compute the correlation between the IPO value at that lead time and the ice-free year relative to the ensemble-mean ice-free year (even if the ensemble member is already ice-free for a given lead time).

**Table 1.** List of Global Climate Models used, listed with the number of ensemble members that have the data necessary for calculating all pertinent analysis metrics. SIA Sept shows the historical mean September sea ice area over 1979–1998 (million $km^2$) as reported in Notz and SIMIP-Community (2020). dSIA / dGMST refers to a measure of the forced response (million $km^2$ $°C^{-1}$) as reported in Notz and SIMIP-Community (2020). A * next to these two metrics indicates that models and observational estimates ($5.97 \pm 0.66$ for Sept SIA and $-4.01 \pm 0.32$ for dSIA / dGMST, Notz and SIMIP-Community, 2020) overlap within the uncertainty ranges. IPO skill refers to the ranking of skill score computed by Qin et al. (2024) for regressed distribution of sea surface temperature on the IPO compared with observations. Note EC-Earth3 is recorded as N/A as it was not assessed in Qin et al. (2024).

| Modeling Center | Model Name | # | Sept SIA | dSIA / dGMST | IPO Skill | CMIP era | Citation |
|---|---|---|---|---|---|---|---|
| CSIRO | ACCESS-ESM1-5 | 40 | $5.19 \pm 0.25$* | $-1.87 \pm 0.27$ | 46th/52 | CMIP6 | Ziehn et al. (2020) |
| CCCma | CanESM5 | 49 | $6.78 \pm 0.26$* | $-2.32 \pm 0.28$ | 21st/52 | CMIP6 | Swart et al. (2019) |
| NCAR | CESM2-LENS | 50 | $4.25 \pm 0.42$ | $-3.72 \pm 0.44$* | 1st/52 | CMIP6 | Danabasoglu et al. (2020) |
| SMHI | EC-Earth3 | 50 | $6.56 \pm 1.06$* | $-2.65 \pm 0.64$ | N/A | CMIP6 | Wyser et al. (2021) |
| MIROC | MIROC6 | 50 | $5.35 \pm 0.21$* | $-2.24 \pm 0.42$ | 23rd/52 | CMIP6 | Shiogama et al. (2023) |
| MPI | MPI-ESM1-2-LR | 30 | $4.44 \pm 0.2$ | $-1.95 \pm 0.42$ | 34th/52 | CMIP6 | Mauritsen et al. (2019) |
| CCCma | CanESM2 | 50 | $3.18 \pm 0.06$ | $-1.76 \pm 0.23$ | 25th/52 | CMIP5 | Kirchmeier-Young et al. (2017) |
| NCAR | CESM1 | 40 | $6.24 \pm 0.12$* | $-2.89 \pm 0.24$ | 12th/52 | CMIP5 | Kay et al. (2015) |

## 3 Results and discussion

### 3.1 Ice-free trajectories and the IPO

The initial phase of the IPO is only statistically significant in affecting trajectories of September sea ice extent (SIE) for 3 of the 8 large ensembles (LEs). Following the methodology by Screen and Deser (2019) for CESM1, significant differences in SIE are also found for MPI-ESM1-2-LR and EC-Earth3 (see Fig. 1). For both CESM1 and MPI-ESM1-2-LR the initially negative phase of the IPO produces lower SIE when compared with trajectories which start with an initially positive phase of the IPO. EC-Earth3, in contrast, simulates lower SIE trajectories when the initial positive phase of the IPO occurs. Thus, there is little consensus between the LEs on the predictive skill of the IPO alone in determining SIE trajectories towards a consistently ice-free Arctic, when following the methodology of Screen and Deser (2019). In fact, it is only the CESM1 (as used in Screen and Deser, 2019) that shows significantly diverging trajectories when ensemble-mean ice-free conditions first occur and for a continuous period of over a decade.

Broadening the analysis of the IPO's influence from one initial mean state to the average of 11 mean states, and defining IPO phase based on 10 years of sign persistence (see Sect. 2.2), significant sea ice trajectory divergence due to the initial IPO phase increases to 6 of the 8 LEs (see Fig. 2a). Now only CanESM2 and CanESM5 do not show any significant impact of the IPO on the trajectory of Arctic SIE decline from initial mean states similar to today. However, even for the LEs that now show significant trajectory divergence, this divergence occurs at different times. CESM2-LENS and MPI-ESM1-2-LR significantly diverge during the first decade following 10 years of IPO phase persistence, whereas CESM1, EC-Earth3, ACCESS-ESM1-5, and MIROC6 diverge in the second decade. However, significant trajectory divergence does not usually coincide with the period close to consistently ice-free conditions in the respective ensemble means (25–51 years), reducing the utility of the present-day IPO phase to reduce consistently ice-free projection uncertainty. Exclusively looking at the timing of a consistently ice-free Arctic (shown numerically and as vertical lines in Fig. 2a), we find all LEs experience earlier ice-free conditions for the initially negative IPO phase ensemble members compared with the ensemble mean, with the exception of EC-Earth3. However, only CESM1 and CESM2-LENS exhibit significantly earlier ice-free conditions for initially negative phases of the IPO compared with the positive IPO ensemble member mean. As before, EC-Earth3 responds strongly in the opposite direction and has significantly later consistently ice-free conditions for the initially negative IPO member compared with the initially positive IPO members.

Notably, during the period 17–22 years of the trajectories, there is clear spatial evidence of the influence of initial IPO phase across the LEs. For six of the eight LEs, a majority of the Central Arctic has a significant anomaly relative to the ensemble mean for at least one of the initial IPO phases for the 17–22 year lead time (Fig. 2d, e). The two exceptions, CanESM5 and CESM2-LENS, differ in nature. CanESM5 shows no significant IPO influence on sea ice in any analysis presented here. CESM2-LENS, by contrast, shows a significant influence of the IPO on both SIE trajectories and ice-free timing, making its lack of a significant 17–22 year SIC signal notable. For CESM2-LENS this lead-time window corresponds to 2009–2030 in 96 % of ensemble trajectories, which overlaps with the anomalous forced sea ice evolution in CESM2 driven by its sensitivity to biomass-burning aerosol emissions (DeRepentigny et al., 2022). This transient forced signal may obscure the internal IPO-driven SIC anomaly in the composite, offering a possible explanation for the muted response in an otherwise IPO-sensitive model.

At the 2–7 year time period, however, widespread SIC anomalies are not found (Fig. 2b, c), indicating that the per-

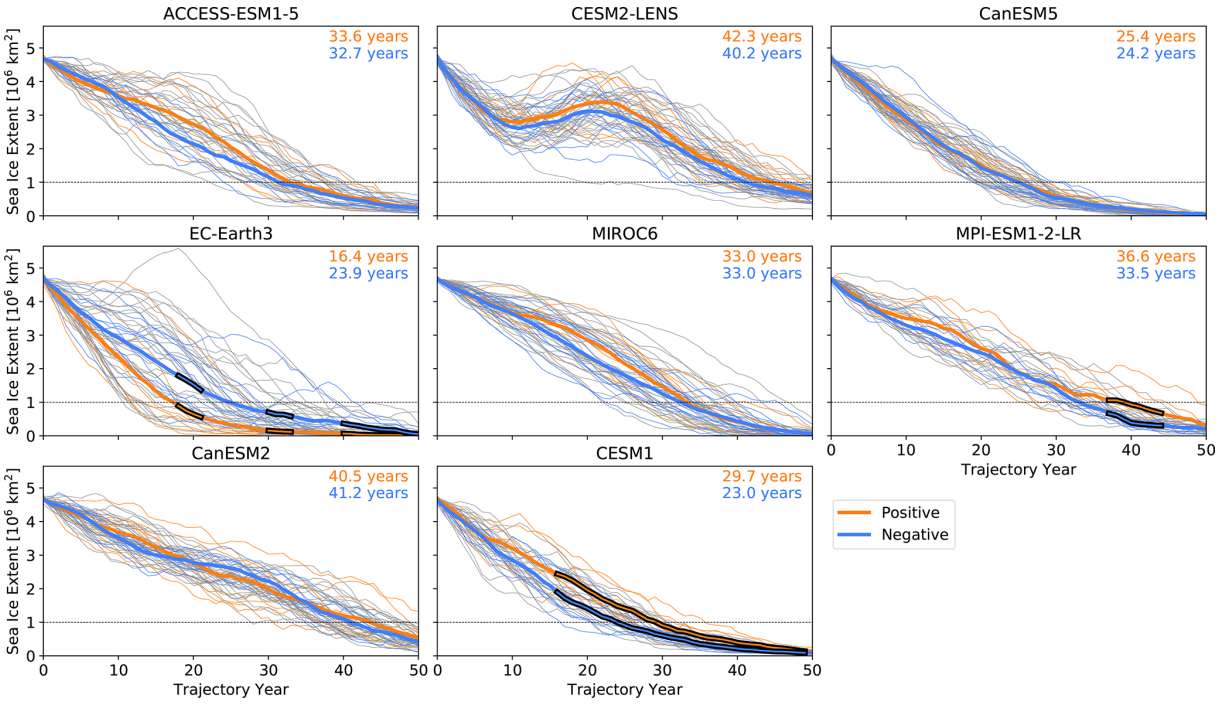



**Figure 1.** September mean SIE trajectories starting at 4.7 million km$^2$, categorized based on initial IPO phase with a threshold of 0.9 $\sigma$, following Screen and Deser (2019). The thin orange lines indicate trajectories where the initial IPO exceeds 0.9 $\sigma$ and the bold orange line is the average of the positive IPO trajectories. Similarly the blue lines are for initial IPO values of $-0.9$ $\sigma$ and lower, grey indicates trajectories with an initially neutral IPO phase. The numbers in the top right of each subplot indicate the average trajectory year before consistently ice-free conditions for the average trajectory starting with a positive or negative IPO phase. Periods where the IPO phase trajectory averages are significantly different from one another are bounded in black.

sistence of the IPO phase for 10 years has a limited impact on near-term sea ice trajectories. The IPO phase transition varies considerably between models and ensemble members, but commonly occurs between the 2–7 and 17–22 lead time windows. The IPO phase transition was suggested as the mechanism for delaying or hastening consistently ice-free conditions in CESM1 (Screen and Deser, 2019). As there is broad symmetry in the SIC composites at 17–22 years for opposite initial IPO phases (aside from the CanESM LEs), we may be able to consider the initial IPO sign as correlated to regions of enhanced or muted melting. However, as the significant SIE divergence between initial IPO phases is often strongest at approximately a two decade lead time, the IPO may only become an important driver once we are closer to consistently ice-free conditions than the current 32-year multi-model mean duration. In Sect. 3.2 we thus assess whether the IPO becomes a better timing signal at shorter lead times to ice-free conditions, and whether the strength of the IPO is related to how early or late consistently ice-free conditions can be expected.

### 3.2 IPO Strength and Ice-Free Timing

Despite the significant impact of the IPO phase on sea ice concentration two decades from similar mean states as today, no model except CESM1 shows a significant correlation between the IPO at a two-decade lead time and the timing of consistently ice-free conditions. Across the LEs, no common lead time shows a significant correlation, and in most LEs no significant correlation exists at any lead time up to the 45 years examined (Fig. 3A–H). Additionally, there is no agreement between the LEs on the sign of the correlation close to ice-free conditions, at 4.7 million km$^2$ (vertical lines in Fig. 3A–H), or at longer lead-times. This inconsistency argues against a specific physical mechanism linking IPO phase to ice-free timing, which would instead be expected to produce a correlation that peaks at a characteristic lead time and decays elsewhere. The alternating correlation sign seen in EC-Earth3 and MPI-ESM1-2-LR is consistent with the IPO's typical two-to-three decade phase changes, but this pattern is not shared across other models.

Looking at shorter lead times to consistently ice-free conditions than where we are today, we find that five of the eight LEs have isolated correlations between the IPO and ice-free timing which are significant at the 0.05 level. However, aside from 3 lagged periods in CESM1 (Fig. 3H), these isolated instances are consistent with what we would expect from chance alone for a sample of 46 correlations computed yearly, following the Benjamini and Hochberg (1995)

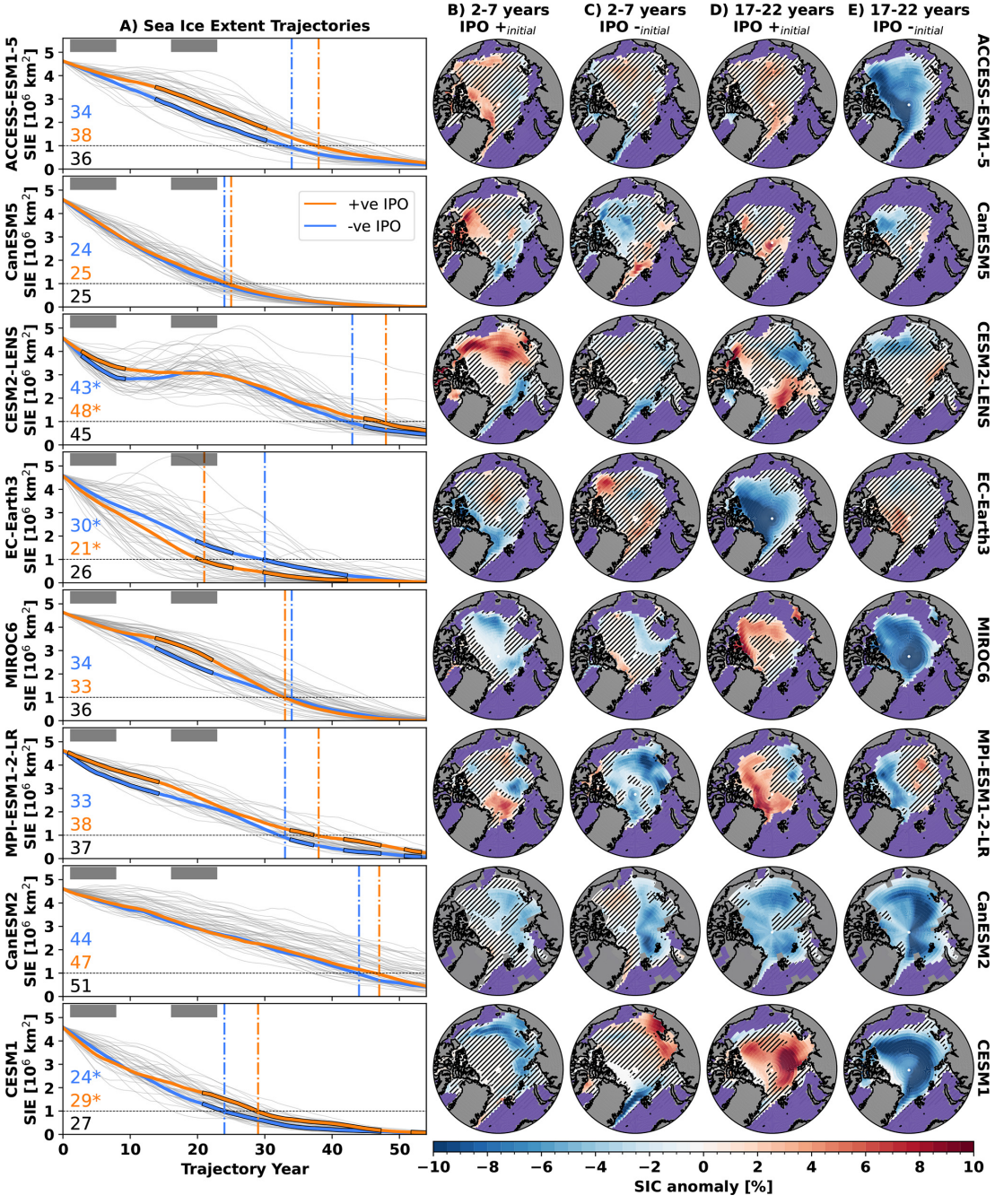



**Figure 2.** Sea ice trajectories categorized by initial IPO phase. **(A)** The September SIE trajectories from 11 initial SIE states of 4.2–5.2 million km$^2$ selected based on persistence of the IPO in a positive or negative phase for at least 10 years. When the two trajectories are statistically different from one another they are bounded in black. Light gray lines indicate the individual ensemble members. The printed numbers near the origin indicate the number of years before consistently ice-free conditions for the pooled trajectories (* for significantly different from one another) and, in black, the ensemble mean. Grey boxes at the top of the subplots indicate the temporal period for which the spatial plots **(B)**–**(E)** are averaged. **(B, C)** September sea ice concentration anomalies in years 2 to 7 of the trajectories relative to the ensemble mean, for initially positive **(B)** and negative **(C)** IPO phases. **(D)** and **(E)** is the same as **(B)** and **(C)** except for the averaging period of 17 to 22 years. Hatching indicates regions of sea ice anomaly which do not meet the 0.05 significance threshold. Purple shaded regions indicate open ocean where no ensemble member exceeds 15 % concentration over the time period.

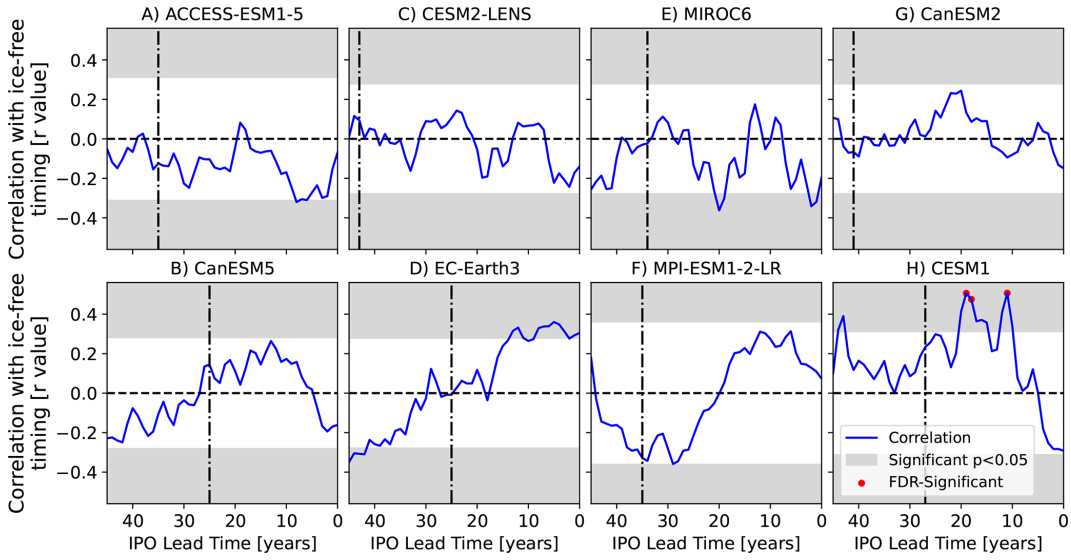



**Figure 3.** Significance of correlations between the IPO and early or late consistently ice-free conditions in September at up to 45-year lead times. Pearson $r$-value shown as a blue line for the correlation between consistently ice-free year for each member relative to the ensemble mean, and the initial value of the IPO for each ensemble member at a given number of years before ensemble mean ice-free conditions. Vertical dashed lines indicates the ensemble mean duration between 4.7 million km$^2$ and consistently ice-free conditions. Grey shading indicates the threshold for a significant correlation for the ensemble member size, with red dots indicating lags for which the correlation remains significant following a Benjamini-Hochberg false discovery procedure.

false discovery rate ($\alpha = 0.05$). Only CESM1 shows correlations which are highly unlikely to occur due to random chance, with a strongest correlation at a 19-year lead time ($p = 0.001$). Where correlations are significant, both positive and negative IPO phases show a broadly symmetrical response, indicating that the relationship is not driven by one phase alone. This symmetry suggests that even though the relationship between the IPO and ice-free timing is weak when considered across the full range of IPO values, predictability could emerge when comparing only the very strongest positive and negative IPO values. MIROC6 was previously identified as having a weak Pacific-Arctic teleconnection (Jahfer et al., 2024), yet it still shows a significant correlation between IPO phase and SIE trajectories at a 20-year lead time. This indicates that modeled Pacific-Arctic teleconnections and the modeled impact of the IPO on consistently ice-free conditions are not necessarily the same thing.

## 4 Conclusions

Beginning from a specific initial sea ice extent (SIE) similar to today, we find that only one model (CESM1) of the eight large ensembles (LEs) studied shows a statistically significant impact of the initial IPO phase on SIE trajectories leading up to consistently ice-free conditions. This demonstrates that the strong impact of the IPO on the timing of consistently ice-free conditions as reported in Screen and Deser (2019) is not replicated beyond the CESM1 model. When we increase our sample size to 11 initial starting SIEs (pooling), to remove the dependence on the specific starting SIE, we do find that CESM2-LENS also shows statistically significantly earlier ice-free conditions with an initially negative phase of the IPO. EC-Earth3 also shows a statistically significant effect of the IPO on ice-free conditions, but in the opposite direction of the CESM models, with later consistently ice-free conditions for an initially negative IPO. However, five of the eight LEs show no statistically significant impact of initial IPO phase on the timing of consistently ice-free conditions. Thus, there is currently no consensus on the utility of the IPO for determining when consistently ice-free conditions will occur, when assessed from September mean SIEs between 4.2–5.2 million km$^2$.

Lacking model consensus, can we determine which model is the most realistic in capturing the processes involved? Unfortunately, the currently available realism metrics (see Table 1) cannot clearly determine which model, if any, is most realistic in capturing all processes involved. Qin et al. (2024) place CESM1 and CESM2-LENS in the upper quartile for IPO spatial realism (EC-Earth3 was not assessed), and CanESM5, CanESM2, and MIROC6 in the upper half (see Table 1). Jahfer et al. (2024) classify all CMIP6 models except MIROC6 as having a strong Pacific–Arctic teleconnection (CESM1 and CanESM2, the two CMIP5 models, were not assessed). Thus, despite good relevant metrics for several of the models, we see large differences between the spatial and temporal IPO–sea ice responses, making it unlikely that a single common physical mechanism underlies

them. We therefore find insufficient evidence for a single, realistic IPO–ice-free relationship.

While we find no consistent relationship between the initial IPO and consistently ice-free conditions among the LEs, the IPO does appear to have an impact on the trajectory of sea ice decline at a lead time of approximately two decades from current extents. Significantly lower September sea ice concentrations (SIC) in the central Arctic occur at this lead time in four of the eight LEs for an initially negative IPO (six show a significant anomaly for at least one phase), with no LEs indicating significantly higher SICs. Given the current negative phase of the IPO which has persisted since 1998, and has strengthened to $-1.6$ standard deviations in the 11-year window centered on December 2019, SIC loss faster than the forced trend may be expected in two decades. However, the model results show that even if the current IPO phase drives broad changes in the Central Arctic SIC field at around 20 years in the future, this has a weaker impact on the threshold-based SIE. Thus, we find that the IPO does not reliably translate into a useful forecasting tool to reduce internal variability uncertainty of a consistently ice-free Arctic Ocean.

*Code and data availability.* The climate model data is available from https://aims2.llnl.gov/search/cmip5/ (last access: 9 February 2024) for CMIP5 and https://aims2.llnl.gov/search/cmip6/ (last access: 9 February 2024) for CMIP6. The observational sea ice index dataset is available from NSIDC at https://doi.org/10.7265/N5K072F8 (Fetterer et al., 2017). Sea surface temperature dataset HadISST is available from https://doi.org/10.5065/XMYE-AN84 (Hadley Centre for Climate Prediction and Research, 2000). The Tripole Index for the Interdecadal Pacific Oscillation is available from https://psl.noaa.gov/data/timeseries/IPOTPI/ (last access: 18 November 2025). The code used to replicate these analyses is archived with Zenodo (https://doi.org/10.5281/zenodo.24328522, Wyburn-Powell, 2026a). Similarly, the data sets used to reproduce this material is archived with the Arctic Data Center (https://doi.org/10.18739/A2CN6Z23B, Wyburn-Powell, 2026b).

*Author contributions.* CWP contributed data curation, formal analysis, investigation, methodology, visualization, and writing (original draft preparation), AJ contributed funding acquisition, conceptualization, methodology, project administration, supervision, and writing (review and editing).

*Competing interests.* The contact author has declared that neither of the authors has any competing interests.

*Disclaimer.* Publisher's note: Copernicus Publications remains neutral with regard to jurisdictional claims made in the text, published maps, institutional affiliations, or any other geographical representation in this paper. The authors bear the ultimate responsibility for providing appropriate place names. Views expressed in the text are those of the authors and do not necessarily reflect the views of the publisher.

*Acknowledgements.* We acknowledge the World Climate Research Programme, which, through its Working Group on Coupled Modelling, coordinated and promoted CMIP6. We thank the climate modeling groups for producing and making available their model output, the Earth System Grid Federation (ESGF) for archiving the data and providing access, and the multiple funding agencies who support CMIP6 and ESGF. We also acknowledge the US CLIVAR Working Group on Large Ensembles and the modeling centers that contributed to the CLIVAR Large Ensemble project. We would also like to acknowledge high-performance computing on Cheyenne (https://doi.org/10.5065/D6RX99HX) provided by NCAR's Computational and Information Systems Laboratory, sponsored by the National Science Foundation. We also acknowledge helpful feedback from J.E. Kay, M.M. Holland, D.A. Bailey and K.B. Karnauskas as well as from two anonymous reviewers.

*Financial support.* This research has been supported by the National Science Foundation, Directorate for Geosciences (grant no. 1847398).

*Review statement.* This paper was edited by Petra Heil and reviewed by two anonymous referees.

## References

Årthun, M., Onarheim, I. H., Dörr, J., and Eldevik, T.: The Seasonal and Regional Transition to an Ice-Free Arctic, Geophys. Res. Lett., 48, https://doi.org/10.1029/2020GL090825, 2021.

Baxter, I., Ding, Q., Schweiger, A., L'Heureux, M., Baxter, S., Wang, T., Zhang, Q., Harnos, K., Markle, B., Topal, D., and Lu, J.: How tropical Pacific surface cooling contributed to accelerated sea ice melt from 2007 to 2012 as ice is thinned by anthropogenic forcing, J. Climate, 32, 8583–8602, https://doi.org/10.1175/JCLI-D-18-0783.1, 2019.

Benjamini, Y. and Hochberg, Y.: Controlling the False Discovery Rate: a Practical and Powerful Approach to Multiple Testing, J. R. Stat. Soc., 57, 289–300, 1995.

Bonan, D. B. and Blanchard-Wrigglesworth, E.: Nonstationary Teleconnection Between the Pacific Ocean and Arctic Sea Ice, Geophys. Res. Lett., 47, https://doi.org/10.1029/2019GL085666, 2020.

Bonan, D. B., Lehner, F., and Holland, M. M.: Partitioning uncertainty in projections of Arctic sea ice, Environ. Res. Lett., 16, https://doi.org/10.1088/1748-9326/abe0ec, 2021.

Danabasoglu, G., Lamarque, J. F., Bacmeister, J., Bailey, D. A., DuVivier, A. K., Edwards, J., Emmons, L. K., Fasullo, J., Garcia, R., Gettelman, A., Hannay, C., Holland, M. M., Large, W. G., Lauritzen, P. H., Lawrence, D. M., Lenaerts, J. T., Lindsay, K., Lipscomb, W. H., Mills, M. J., Neale, R., Oleson, K. W., Otto-Bliesner, B., Phillips, A. S., Sacks, W., Tilmes, S., van Kampenhout, L., Vertenstein, M., Bertini, A., Dennis, J., Deser, C., Fis-

cher, C., Fox-Kemper, B., Kay, J. E., Kinnison, D., Kushner, P. J., Larson, V. E., Long, M. C., Mickelson, S., Moore, J. K., Nienhouse, E., Polvani, L., Rasch, P. J., and Strand, W. G.: The Community Earth System Model Version 2 (CESM2), J. Adv. Model. Earth Sys., 12, https://doi.org/10.1029/2019MS001916, 2020.

DeRepentigny, P., Jahn, A., Holland, M. M., Kay, J. E., Fasullo, J., Lamarque, J.-F., Tilmes, S., Hannay, C., Mills, M. J., Bailey, D. A., and Barrett, A. P.: Enhanced simulated early 21st century Arctic sea ice loss due to CMIP6 biomass burning emissions, Sci. Adv., 8, 2405, https://doi.org/10.1126/sciadv.abo2405, 2022.

Ding, Q., Wallace, J. M., Battisti, D. S., Steig, E. J., Gallant, A. J., Kim, H. J., and Geng, L.: Tropical forcing of the recent rapid Arctic warming in northeastern Canada and Greenland, Nature, 509, 209–212, https://doi.org/10.1038/nature13260, 2014.

Fasullo, J. T., Phillips, A. S., and Deser, C.: Evaluation of Leading Modes of Climate Variability in the CMIP Archives, J. Climate, 33, 5527–5545, https://doi.org/10.1175/jcli-d-19-1024.1, 2020.

Fetterer, F., Knowles, K., Meier, W. N., Savoie, M., and Windnagel, A. K.: Sea Ice Index (G02135, Version 3), National Snow and Ice Data Center Boulder [data set], https://doi.org/10.7265/N5K072F8, 2017.

Hadley Centre for Climate Prediction and Research, Met Office, Ministry of Defence, United Kingdom: Hadley Centre Global Sea Ice and Sea Surface Temperature (HadISST), NSF National Center for Atmospheric Research [data set], https://doi.org/10.5065/XMYE-AN84, 2000.

Henley, B. J., Gergis, J., Karoly, D. J., Power, S., Kennedy, J., and Folland, C. K.: A Tripole Index for the Interdecadal Pacific Oscillation, Clim. Dynam., 45, 3077–3090, https://doi.org/10.1007/s00382-015-2525-1, 2015.

Holland, B. M. M. and Hunke, E. C.: A Review of Arctic Sea Ice Climate Predictability in Large-Scale Earth System Models, Oceanography, 35, 20–27, https://doi.org/10.5670/oceanog.2022.113, 2022.

Jahfer, S., Ha, K.-J., Chung, E.-S., Franzke, C. L. E., and Sharma, S.: Unveiling the role of tropical Pacific on the emergence of ice-free Arctic projections, Environ. Res. Lett., 19, 044033, https://doi.org/10.1088/1748-9326/ad3141, 2024.

Jahn, A., Kay, J. E., Holland, M. M., and Hall, D. M.: How predictable is the timing of a summer ice-free Arctic?, Geophys. Res. Lett., 43, 9113–9120, https://doi.org/10.1002/2016GL070067, 2016.

Jahn, A., Holland, M., and Kay, J.: Projections of an ice-free Arctic Ocean, Nat. Rev. Earth Environ., 5, 164–176, https://doi.org/10.1038/s43017-023-00515-9, 2024.

Kay, J. E., Holland, M. M., and Jahn, A.: Inter-annual to multi-decadal Arctic sea ice extent trends in a warming world, Geophys. Res. Lett., 38, 2–7, https://doi.org/10.1029/2011GL048008, 2011.

Kay, J. E., Deser, C., Phillips, A., Mai, A., Hannay, C., Strand, G., Arblaster, J. M., Bates, S. C., Danabasoglu, G., Edwards, J., Holland, M., Kushner, P., Lamarque, J. F., Lawrence, D., Lindsay, K., Middleton, A., Munoz, E., Neale, R., Oleson, K., Polvani, L., and Vertenstein, M.: The community earth system model (CESM) large ensemble project: A community resource for studying climate change in the presence of internal climate variability, B. Am. Meteorol. Soc., 96, 1333–1349, https://doi.org/10.1175/BAMS-D-13-00255.1, 2015.

Kim, H., Yeh, S. W., An, S. I., and Song, S. Y.: Changes in the role of Pacific decadal oscillation on sea ice extent variability across the mid-1990s, Sci. Rep., 10, https://doi.org/10.1038/s41598-020-74260-0, 2020.

Kirchmeier-Young, M. C., Zwiers, F. W., and Gillett, N. P.: Attribution of extreme events in Arctic Sea ice extent, J. Climate, 30, 553–571, https://doi.org/10.1175/JCLI-D-16-0412.1, 2017.

Mauritsen, T., Bader, J., Becker, T., Behrens, J., Bittner, M., Brokopf, R., Brovkin, V., Claussen, M., Crueger, T., Esch, M., Fast, I., Fiedler, S., Fläschner, D., Gayler, V., Giorgetta, M., Goll, D. S., Haak, H., Hagemann, S., Hedemann, C., Hohenegger, C., Ilyina, T., Jahns, T., de-la Cuesta, D. J., Jungclaus, J., Kleinen, T., Kloster, S., Kracher, D., Kinne, S., Kleberg, D., Lasslop, G., Kornblueh, L., Marotzke, J., Matei, D., Meraner, K., Mikolajewicz, U., Modali, K., Möbis, B., Müller, W. A., Nabel, J. E., Nam, C. C., Notz, D., Nyawira, S. S., Paulsen, H., Peters, K., Pincus, R., Pohlmann, H., Pongratz, J., Popp, M., Raddatz, T. J., Rast, S., Redler, R., Reick, C. H., Rohrschneider, T., Schemann, V., Schmidt, H., Schnur, R., Schulzweida, U., Six, K. D., Stein, L., Stemmler, I., Stevens, B., von Storch, J. S., Tian, F., Voigt, A., Vrese, P., Wieners, K. H., Wilkenskjeld, S., Winkler, A., and Roeckner, E.: Developments in the MPI-M Earth System Model version 1.2 (MPI-ESM1.2) and Its Response to Increasing $CO_2$, J. Adv. Model. Earth Sy., 11, 998–1038, https://doi.org/10.1029/2018MS001400, 2019.

Notz, D.: How well must climate models agree with observations?, Philos. T. R. Soc. A, 373, https://doi.org/10.1098/rsta.2014.0164, 2015.

Notz, D. and SIMIP-Community: Arctic Sea Ice in CMIP6, Geophys. Res. Lett., 47, https://doi.org/10.1029/2019GL086749, 2020.

Phillips, A., Deser, C., and Fasullo, J.: A New Tool for Evaluating Modes of Variability in Climate Models, Eos, 95, 453–455, https://doi.org/10.1002/2014EO490002, 2014.

Qin, Z., Wang, T., Chen, H., and Gao, Y.: Performance of CMIP5 and CMIP6 models in reproducing the Interdecadal Pacific Oscillation and its global impacts, Int. J. Climatol., 44, 3742–3765, https://doi.org/10.1002/joc.8548, 2024.

Rayner, N. A., Parker, D. E., Horton, E. B., Folland, C. K., Alexander, L. V., Rowell, D. P., Kent, E. C., and Kaplan, A.: Global analyses of sea surface temperature, sea ice, and night marine air temperature since the late nineteenth century, J. Geophys. Res.-Atmos., 108, 4407, https://doi.org/10.1029/2002jd002670, 2003.

Screen, J. A. and Deser, C.: Pacific Ocean Variability Influences the Time of Emergence of a Seasonally Ice-Free Arctic Ocean, Geophys. Res. Lett., 46, 2222–2231, https://doi.org/10.1029/2018GL081393, 2019.

Shiogama, H., Tatebe, H., Hayashi, M., Abe, M., Arai, M., Koyama, H., Imada, Y., Kosaka, Y., Ogura, T., and Watanabe, M.: MIROC6 Large Ensemble (MIROC6-LE): experimental design and initial analyses, Earth Syst. Dynam., 14, 1107–1124, https://doi.org/10.5194/esd-14-1107-2023, 2023.

Simon, A., Gastineau, G., Frankignoul, C., Lapin, V., and Ortega, P.: Pacific Decadal Oscillation modulates the Arctic sea-ice loss influence on the midlatitude atmospheric circulation in winter, Weather Clim. Dynam., 3, 845–861, https://doi.org/10.5194/wcd-3-845-2022, 2022.

Swart, N. C., Fyfe, J. C., Hawkins, E., Kay, J. E., and Jahn, A.: Influence of internal variability on Arctic sea-ice trends, Nat. Clim. Chang., 5, 86–89, https://doi.org/10.1038/nclimate2483, 2015.

Swart, N. C., Cole, J. N. S., Kharin, V. V., Lazare, M., Scinocca, J. F., Gillett, N. P., Anstey, J., Arora, V., Christian, J. R., Hanna, S., Jiao, Y., Lee, W. G., Majaess, F., Saenko, O. A., Seiler, C., Seinen, C., Shao, A., Sigmond, M., Solheim, L., von Salzen, K., Yang, D., and Winter, B.: The Canadian Earth System Model version 5 (CanESM5.0.3), Geosci. Model Dev., 12, 4823–4873, https://doi.org/10.5194/gmd-12-4823-2019, 2019.

Topál, D., Ding, Q., Mitchell, J., Baxter, I., Herein, M., Haszpra, T., Luo, R., and Li, Q.: An internal atmospheric process determining summertime Arctic sea ice melting in the next three decades: Lessons learned from five large ensembles and multiple CMIP5 climate simulations, J. Climate, 33, 7431–7454, https://doi.org/10.1175/JCLI-D-19-0803.1, 2020.

Vance, T. R., Kiem, A. S., Jong, L. M., Roberts, J. L., Plummer, C. T., Moy, A. D., Curran, M. A., and van Ommen, T. D.: Pacific decadal variability over the last 2000 years and implications for climatic risk, Commun. Earth Environ., 3, https://doi.org/10.1038/s43247-022-00359-z, 2022.

Wettstein, J. J. and Deser, C.: Internal variability in projections of twenty-first-century Arctic sea ice loss: Role of the large-scale atmospheric circulation, J. Climate, 27, 527–550, https://doi.org/10.1175/JCLI-D-12-00839.1, 2014.

Wyburn-Powell, C.: chrisrwp/ice-free: v1.0.0 (Version v1.0.0), Zenodo [code], https://doi.org/10.5281/zenodo.24328523, 2026a.

Wyburn-Powell, C.: Interdecadal Pacific Oscillation and Arctic sea ice concentration and extent data for large ensemble global climate models, Arctic Data Center [data set], https://doi.org/10.18739/A2CN6Z23B, 2026b.

Wyburn-Powell, C. and Jahn, A.: Large-Scale Climate Modes Drive Low-Frequency Regional Arctic Sea Ice Variability, J. Climate, 37, 4313–4333, https://doi.org/10.1175/JCLI-D-23, 2024.

Wyser, K., Koenigk, T., Fladrich, U., Fuentes-Franco, R., Karami, M. P., and Kruschke, T.: The SMHI Large Ensemble (SMHI-LENS) with EC-Earth3.3.1, Geosci. Model Dev., 14, 4781–4796, https://doi.org/10.5194/gmd-14-4781-2021, 2021.

Ziehn, T., Chamberlain, M. A., Law, R. M., Lenton, A., Bodman, R. W., Dix, M., Stevens, L., Wang, Y. P., and Srbinovsky, J.: The Australian Earth System Model: ACCESS-ESM1.5, Journal of Southern Hemisphere Earth Systems Science, 70, 193–214, https://doi.org/10.1071/ES19035, 2020.